Controller Design of a MEMS Gyro-Accelerometer with a Single Proof Mass

Woon-Tahk Sung, Taesam Kang*, and Jang Gyu Lee

Abstract: This paper presents a parametric study on the controller design scheme for a gyro-accelerometer to have robust performance under some parameter variations. In particular, an integral and derivative based controller design method is suggested to achieve the desired performances of stability margin, bandwidth, and uniformity of scale for both gyroscopes and accelerometers with uncertainties of quality factor and resonant frequency. The simulation result shows that the control loop based on the suggested method gives satisfactory performance robustness under parameter variations, demonstrating the usefulness of the proposed design scheme.

Keywords: Accelerometer, gyro-accelerometer, gyroscope, MEMS, PID control.

1. INTRODUCTION

Great advances in micro-electromechanical system (MEMS) technologies enable researchers to develop smaller and lighter inertial sensors that are highly useful for various areas. Important applications of such inertial sensors include inertial navigation systems (INS), automotive applications, and consumer devices. MEMS sensors have various advantageous properties such as miniature size, low power consumption, high rigidity, and easy fabrication with low cost by mass-production processes.

Among these properties, the size of the sensor is crucial in practical applications. If the size of a device becomes smaller, the area of its applications can be expanded considerably. The multi-sensor with single-structure is one of the solutions to reducing the size of sensors. Various papers have been published in terms of a multi-axis sensing scheme for accelerometers [1-3] and gyroscopes [4-6], and in terms of a multi-measurement sensing scheme for gyro-accelerometers [7-9]. In the case of multi-axis sensors, it is easy to design the signal processing circuit because of its nearly identical setup for each axis. However, the multi-axis sensors often have large cross-axis sensitivities since their operating frequencies are in the same frequency region, which is an undesirable feature for inertial sensors. On the other hand, the gyro-accelerometer as a multi-measurement system has different operating frequencies for a gyroscope and an accelerometer, thus it has better capability of reducing the cross-axis sensitivity. In this paper, we adopt a gyro-accelerometer as a part of size reduction and suggest a new control method for performance enhancement of the sensor.

The performance of the MEMS gyro-accelerometer is normally affected by its manufacturing errors, e.g. irregularity of thickness, width, and vacuum level, which are the sources of uncertainties in parameters such as resonant frequency and quality factor. Therefore, a control scheme is needed to guarantee the performance under those uncertainties. In this study, we propose a controller design scheme that considers different operating principles of the gyro and the accelerometer. The force-rebalance control is used both for the gyro and the accelerometer to achieve performance goals by force feedback loop that regulates the motion of proof mass in some limited level. With this control scheme, we can achieve performance goals both for the gyro and the accelerometer under some uncertainties in system parameters.

2. SYSTEM ILLUSTRATION

2.1. Operational principle

Mechanical model of a gyro-accelerometer in this

Manuscript received July 5, 2007; revised April 7, 2008; accepted June 16, 2008. Recommended by Editorial Board member Hyo-Choong Bang the direction of Editor Hyun Seok Yang. This work was supported by Defense Acquisition Program Administration and the Agency for Defense Development under the contract ADD-07-07-03 and partially supported by Korea Research Foundation Grant KRF-2006-005-J03303.

Woon-Tahk Sung is with Samsung Electronics Co., LTD., Dong Suwon P.O. BOX 105, 416, Maetan-3dong, Yeoong tong-gu, Suwon-si, Gyeonggi-do 443-742, Korea (e-mail: tahk1@snu.ac.kr).

Taesam Kang is with the Department of Aerospace Information Engineering, Konkuk University, Hwayang-dong, Gwangjin-gu, Seoul 143-701, Korea (e-mail: tskang@konkuk.ac.kr).

Jang Gyu Lee is with the School of Electrical Engineering and Computer Science, Seoul National University, Korea (e-mail: jgl@snu.ac.kr).

*Corresponding author.

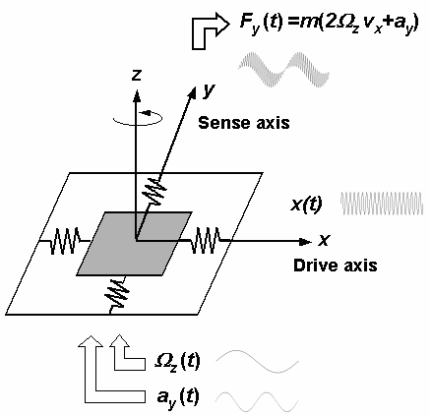

Fig. 1. Mechanical model of MEMS gyro-accelerometer.

study can be depicted as in Fig. 1. The proof mass is sustained by four springs and the motion is constrained along the x- and y-axis by making the spring stiffness of the z-axis very large. Then, the proof mass can be modeled as a mass-spring-damper system with two degrees of freedom. The x-axis is a drive axis to induce drive-oscillation of the gyroscope whose frequency is set to be identical with the resonant frequency of the drive mode in order to create a large oscillating motion with the smallest energy. Coriolis acceleration induced by z-axis angular rate input and the linear acceleration input along y-axis together induce the mass to oscillate along the y-axis.

If we measure the control force that regulates this oscillation using a control loop, then we can estimate the input angular rate and linear acceleration at the same time by filtering and demodulating the control signal. Since the oscillating motion along the y-axis due to the Coriolis acceleration is modulated by the driving signal, the demodulation process is essentially needed to extract the original signal. A linear acceleration to the y-axis, on the other hand, is directly measured by low-pass filtering of the control signal.

2.2. Dynamic equations

The equation of motion of a MEMS gyro-accelerometer can be expressed as a lumped mass-spring-damper system operating in its first two fundamental in-plane modes, i.e., drive and sense modes as in the following equation:

$$\begin{aligned} m_x\ddot{x} + d_{xx}\dot{x} + k_{xx}x &= f_x, \\ m_y\ddot{y} + d_{yy}\dot{y} + k_{yy}y &= f_y \end{aligned} \tag{1}$$

and f_x, f_y in (1) are equal to

$$\begin{aligned} f_x &= d_{xy}\dot{y} + k_{xy}y + 2m_y\Omega_z\dot{y} + m_x a_x + f_d, \\ f_y &= d_{yx}\dot{x} + k_{yx}x + 2m_x\Omega_z\dot{x} + m_y a_y - f_c, \end{aligned} \tag{2}$$

where f_x and f_y are the overall force at each axis and m_x, m_y, d_{xx}, d_{yy} and k_{xx}, k_{yy} are damping and spring coefficients for x and y axis, Ω_z is the angular velocity components along z-axis and f_d, f_c are driving force and control force that we apply in the control loop. The a_x and the a_y represent the accelerations applied to the proof mass along the x axis and y axis, respectively. In this equation, the cross-axis term k_{xy}, k_{yx} and d_{xy}, d_{yx} are due to fabrication imperfections, the values of which are hardly identified. If we apply feedback force-rebalance control to keep $y, \dot{y}, \ddot{y}$ negligibly small, we obtain (3) from (2) under the assumption of d_{xy}=d_{yx}=0.

$$\begin{aligned} f_d &= f_x + m_x a_x, \\ f_c &= k_{yx}x + 2m_x\Omega_z\dot{x} + m_y a_y. \end{aligned} \tag{3}$$

In (3), the control force f_c is the sum of three different components: Coriolis force, inertial force due to y-axis linear acceleration, and coupling term by x-axis cross sensitivity. The Coriolis and linear acceleration terms can be easily separated by low pass filtering. However, the Coriolis term and coupling term have identical frequency components, and we cannot separate these two terms by the direct filtering process. For these two terms, noting that $x(t)$ is a sinusoidal signal and the phase difference between the two terms are $\pi/2$, the coupling term can be excluded by phase control in the demodulation process.

3. CONTROL LOOP DESIGN

The design goal of the control loop is to achieve required performances of the gyro and the accelerometer under the condition of parameter variations originated from manufacturing errors. To handle those error factors by appropriate control scheme, the control configuration shown in Fig. 2 is needed. As shown in the figure, the control loops are mainly divided into two parts–driving oscillation loop

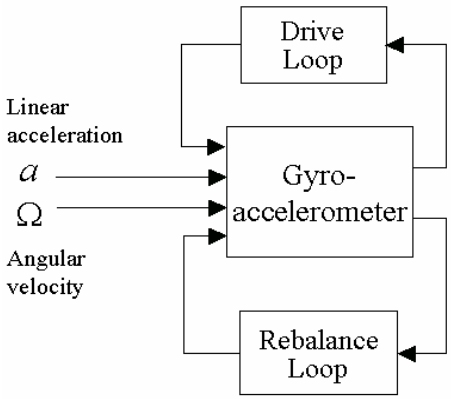

Fig. 2. Block diagram of the drive loop and the force rebalance loop in MEMS gyro-accelerometer.

in drive mode and rebalance loop in sense mode. The drive loop controls the drive mode to oscillate sinusoidally with constant amplitude, while the rebalance loop controls the sense mode oscillation to be kept very small notwithstanding disturbances of angular rate and linear acceleration inputs. The control of the drive loop can be designed using various control methods. The most popular one is automatic gain control (AGC) scheme [10,11]. In this study, we assume that the driving oscillation loop control is already set up, i.e. the oscillation of the proof mass is well sustained under parameter variation of the drive mode [19]. Thus, we focus on the controller design of the sense mode. The design procedure in detail is presented in the following sections.

3.1. Concept of the force-rebalance loop using an integral-derivative control scheme

Force rebalance loop is a closed feedback control loop that enables a sensor to be robust to system uncertainties and to get performance enhancement such as bandwidth and linearity for gyroscope [21,22] as well as accelerometer [23-25]. Various methods of control techniques may be applied to the system. The main issue of the control scheme is that parameters of MEMS structure are apt to have different values due to the manufacturing errors, which can cause severe uncertainty in plant transfer function. For example, MEMS gyroscopes usually can have 10% error in their width of parallel spring due to manufacturing imperfection. This will lead to 15% error in resonant frequency, since the resonant frequency of the proof mass suspended by beam springs can be calculated as follows [12]:

$$\omega_n = \sqrt{\frac{2w^3 hE}{mL}}, \tag{4}$$

where w, h, L are width, height, and length of beam spring, respectively. m is the mass of the structure and E is the modulus of elasticity of the beam material. Therefore, the controller designer should put a focus on handling this uncertainty problem.

Since the MEMS gyro operates at its resonant frequency, the change of resonant frequency can cause large model uncertainty of the plant. The multiplicative uncertainty could be increased to more than a hundred times of the normal uncertainty as the quality factor increases. Therefore, the control scheme that can handle such large uncertainty is needed. Although modern robust control theory such as H_∞ controller has been successfully applied for the problem of robust performance in a sophisticated and structured way, it is hard to design a controller that satisfies the performance specification when the uncertainty is very large, considering that its design

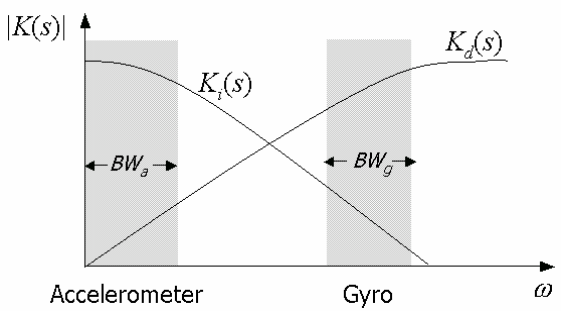

Fig. 3. Operating frequency region of the controller.

procedure is based on the small gain theorem [20]. In this study, we used a classical PID method that can handle the large uncertainty, maintaining the performance. PID control is the most widely used control method in many industrial applications. Not only its simplicity and good capability but also its robustness is an attractive feature to MEMS sensors. Many studies deal with the robustness of PID control in various ways. Most of those studies deal with a reduction of sensitivity function in Nyquist domain [13-15] and gain and phase margin adjustment in bode plot [12,16]. These approaches are useful in many applications because shaping of sensitivity function (and complementary sensitivity function) is directly related to robust stability and robust performance. But in many cases, it deals with the case of small uncertainty. Moreover, the sensitivity specification does not directly reveal the specified performances like bandwidth. We present, in this paper, the parameter tuning of PID controller based on given mechanical properties and performance specifications. The realization methods of PID controller are usually P, PI, PD, or PID control, all of which are dependent on control purposes. For the gyro-accelerometer, however, we do not use proportional control. Instead, we use the integral-derivative (ID) control scheme since the resonant frequency of the gyro part can be changed by using P control. The ID control can be simply expressed as

$$K(s) = K_i(s) + K_d(s) = \frac{k_i}{s+\tau_i} + \frac{k_d s}{s/\tau_d + 1}, \tag{5}$$

where k_i, and τ_i are gain and time constant for the integral control part and k_d and τ_d are those for the derivative control part. The time constant τ_i in the integral part is employed to prevent saturation of signal by blocking up infinite amplification of DC bias output of the plant, whose value is usually set to be relatively small compared with the bandwidth of the accelerometer. The time constant τ_d in the derivative part is employed to prevent amplification of high frequency noise by restraining large amplification of noise signal whose frequency is

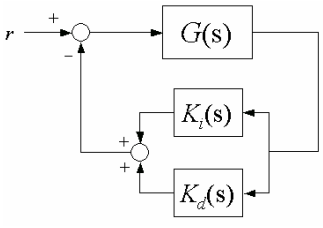

(a) Original loop.

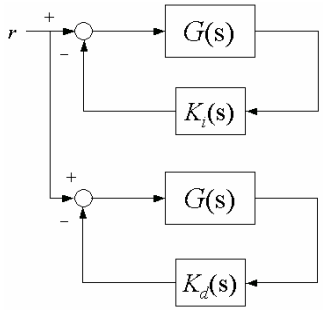

(b) Equivalent two closed loop in ID control.

Fig. 4. Block diagram of closed loop system.

higher than the driving frequency of the gyroscope. Regarding the noise reduction, it is recommended to set τ_d as small as possible, therefore its value is adjusted to be closed to the resonant frequency, considering stability and performance specification. Once the values of τ_i and τ_d are chosen, they can be omitted in the performance analysis for the simplification of calculation.

Since the dominant operating frequency areas of the integral and the derivative controllers are very different, we can analyze the feedback control in separate loop. That is, as long as the transfer function of a gyro-accelerometer is concerned, we can deal with the transfer function as a sum of two transfer functions, since the gain of GK_d is negligible at the frequency area of $\omega \le BW_a$ and GK_i is negligible at $|\omega-\omega_y| \le BW_g$ where ω_y is resonant frequency of the sense mode and BW_a, BW_g are bandwidth of accelerometer and gyroscope as shown in Fig. 3. Therefore, the closed loop transfer function of the system can be approximated as (6), the block diagram of which is illustrated in Fig. 4.

$$\begin{aligned} T &= \frac{GK}{1+GK} = \frac{G\left(K_i+K_d\right)}{1+G\left(K_i+K_d\right)} \\ &= \frac{GK_i}{1+GK_i+GK_d} + \frac{GK_d}{1+GK_i+GK_d} \\ &\approx \left.\frac{GK_i}{1+GK_i}\right|_{\omega \le BW_a} + \left.\frac{GK_d}{1+GK_d}\right|_{|\omega-\omega_y| \le BW_g}, \end{aligned} \tag{6}$$

where $G(s) = 1/(s^2+2\varsigma_y\omega_y s+\omega^2_y)$ is the common factor of the open-loop sense mode transfer functions of the gyro-accelerometer obtained from (1) and (2).

3.2. Integral Gain Adjustment for Performance of the Accelerometer

If we allow the closed loop transfer function of the accelerometer to be

$$\begin{aligned} T_a &\triangleq \frac{GK_i}{1+GK_i} \\ &= \frac{k_i}{s^3+\left(2\zeta_y\omega_y+\tau_i\right)s^2+\left(\omega_y^2+2\zeta_y\omega_y\tau_i\right)s+\omega_y^2\tau_i+k_i} \end{aligned} \tag{7}$$

then, at low frequency, s^3 and s^2 terms can be neglected, which results in an approximated first-order transfer function as follows:

$$T_a \approx \frac{k_i}{\left(\omega_y^2+2\zeta_y\omega_y\tau_i\right)s+k_i+\omega_y^2\tau_i}. \tag{8}$$

(1) Bandwidth: The bandwidth of the accelerometer in (8) can be calculated as a cutoff frequency of a first-order low pass filter. Then, assuming $2\varsigma_y\tau_i << \omega_y$ in usual operation, control gain adjustment based on bandwidth requirement is given as follows:

$$BW_a = \frac{\omega_y^2\tau_i+k_i}{\left(\omega_y^2+2\zeta_y\omega_y\tau_i\right)} \approx \frac{\omega_y^2\tau_i+k_i}{\omega_y^2} \ge BW_{a\_spec}, \tag{9}$$

where BW_{a_spec} is the required specification of the bandwidth of the accelerometer. From condition (9), the condition for k_i is reduced to

$$k_i \ge \omega_y^2\left(BW_{a\_spec}-\tau_i\right). \tag{10}$$

(2) Resolution: The definition of resolution is normally given as the largest value of the minimum change in input to make the output levels greater than those due to noise inputs. In inertial sensors, it is usually considered reasonable to treat this problem in frequency domain. If we consider the feedback system in Fig. 5, the output of the system is the control output u that is given as

$$u = T\cdot r + R\cdot n, \tag{11}$$

where $T = \frac{GK}{1+GK}$, $R = \frac{K}{1+GK}$. Then the resolution of the accelerometer Q_a can be expressed as

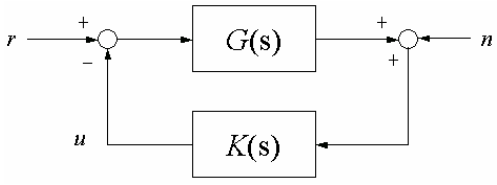

Fig. 5. Rebalance loop with measurement noise.

$$Q_a = \left\{ \min r \left| |T(\omega)\cdot r(\omega)| \geq |R(\omega)\cdot n(\omega)|, \right. \right. \\ \left. \left. \omega < BW_a \right\} \right.$$

The minimum r is achieved at $T \cdot r = R \cdot n$. Then Q_a is obtained as

$$Q_a = \max \frac{R}{T}\cdot n\Big|_{\omega<BW_a} = \max \frac{n}{G}\Big|_{\omega<BW_a}. \quad (12)$$

It is clear that the resolution is not related to the gain of the controller from (12). If we want to have a high resolution, we have to design a high gain plant, i.e., a sensitive structure.

(3) Scale factor uniformity: In addition to the performance enhancement, uniform scale factor is necessary for reliable performance in MEMS sensors. The scale factor uniformity can be investigated by comparison of the transfer function gain. If we allow DC gain of the accelerometer to be

$$A_a = |T_a|_{s=j0} = \frac{k_i}{k_i + \omega_y^2 \tau_i} \quad (13)$$

then the scale factor uniformity can be defined as

$$U_a \triangleq \frac{A_{a\max} - A_{a\min}}{A_{a\max}} = 1 - \frac{k_i + \omega_{y\min}^2 \tau_i}{k_i + \omega_{y\max}^2 \tau_i}, \quad (14)$$

where

$A_{a\max} = \dfrac{k_i}{k_i + \omega_{y\min}^2 \tau_i}$, $A_{a\min} = \dfrac{k_i}{k_i + \omega_{y\max}^2 \tau_i}$. Thus the uniformity criterion $U_a \leq \delta_a$ with respect to the control gain k_i is given as

$$k_i \geq \frac{\tau_i}{\delta_a}\left\{ (1-\delta_a)\omega_{y\max}^2 - \omega_{y\min}^2 \right\}. \quad (15)$$

3.3 Derivative gain adjustment for performance of the gyroscope

The closed loop transfer function of the gyroscope is expressed as:

$$T_g \triangleq \frac{GK_d}{1+GK_d} = \frac{k_d s}{\dfrac{s^3}{\tau_d} + \left(1 + \dfrac{2\zeta_y \omega_y}{\tau_d}\right)s^2 + \left(k_d + 2\zeta_y\omega_y + \dfrac{\omega_y^2}{\tau_d}\right)s + \omega_y^2}. \quad (16)$$

Similar to the accelerometer case, T_g can be approximated as a second-order transfer function like a band pass filter as in (17). The s^3/τ_d term is neglected around and below the resonant frequency region and $2\zeta_y\omega_y/\tau_d \approx 0$ is assumed.

$$T_g \approx \frac{k_d s}{s^2 + \left(k_d + 2\zeta_y\omega_y + \dfrac{\omega_y^2}{\tau_d}\right)s + \omega_y^2} \quad (17)$$

(1) Bandwidth: In second-order band-pass filter like a gyroscope's closed-loop transfer function, the bandwidth is equal to the resonant frequency divided by quality factor, i.e., ω_n/Q or $2\zeta\omega_n$. In the case of the gyroscope, the output is demodulated to the low frequency region and the actual bandwidth of the system in the low frequency is a half of the bandwidth of the original closed-loop transfer function $T_g(s)$. Therefore, from (17), it is calculated as

$$BW_g = \frac{1}{2}\left(BW \text{ of } T_g\right) = \frac{\omega_{T_g}}{2Q_{T_g}} = \frac{k_d + 2\zeta_y\omega_y + \omega_y^2/\tau_d}{2} \geq BW_{g\_spec}, \quad (18)$$

where BW_{g_spec} is required bandwidth for the gyrocope function. As $2\zeta_y\omega_y << \omega_y^2/\tau_d$ in usual syems, applying this assumption to (18), the condition of k_d is given as

$$k_d \geq 2BW_{g\_spec} - \omega_y^2/\tau_d. \quad (19)$$

(2) Resolution: The resolution of the gyroscope can be considered in much the same way as the accelerometer. The only difference is the operating frequency. Therefore, similarly with (12), the value is calculated as

$$Q_g = \max \frac{n}{G}\Big|_{|\omega-\omega_y|<BW_g}. \quad (20)$$

As in the accelerometer case, the resolution is not influenced by the gain of the controller.

Although the resolution is not affected by the controller in theoretic aspects, the noise in actual operation can affect the stability as well as the performance of the system without careful design consideration. Since the control of the gyroscope is a derivative one, the system is apt to be affected by high frequency noise. The variable τ_d is employed to handle this problem, but it might be considered insufficient. For more suppression of high frequency noise, the low-pass filter whose cut-off frequency is several times larger than the gyroscope's resonant frequency can be used. Its effect, however, won't be outstanding if the circuit condition is not too noisy. Moreover, the gyroscope's mechanical dynamics are basically low-pass filter outside of resonant frequency and the demodulation process is rarely influenced by

the noise signal, thus, the employed τ_d in the controller is sufficient in most cases. In addition, the stability of the system can be affected by the inclusion of additional low-pass filter because the poles of the system increase.

(3) Scale factor uniformity: The maximum gain of the gyroscope is achieved at its resonant frequency. If the resonant frequency of the sense mode is different from that of the drive mode, the gain is dramatically reduced in open loop operation because it usually has high quality factor. The force rebalance loop enables the system to have insensitive characteristics over resonant frequency variation. The scale factor uniformity of the gyroscope can be expressed in terms of the gain of the transfer function at resonant peak in the case of matched mode and deviated mode ($\omega_y \leftarrow \omega_y \pm \Delta\omega$). Substitution of $s=j\omega_y$ into (17) leads to the following equation under the assumption of $2\zeta_y\omega_y/\tau_d \approx 0$.

$$A_g = \left|T_g(s)\right|_{s=j\omega_y} = \frac{k_d}{k_d + 2\zeta_y\omega_y + \omega_y^2/\tau_d} \tag{21}$$

The gain at the deviated mode is

$$A_g' = \left|T_g(s)\right|_{\substack{\omega_y \leftarrow \omega_y + \Delta\omega \\ s=j\omega_y}} = \left| \frac{j\omega_y k_d}{2\omega_y\Delta\omega + (\Delta\omega)^2 + j\omega_y\left\{k_d + 2\zeta_y(\omega_y + \Delta\omega) + (\omega_y + \Delta\omega)^2/\tau_d\right\}} \right|. \tag{22}$$

Since the imaginary part of the denominator is much larger than the real part, A_g' can be approximated as

$$A_g' \approx \left| \frac{j\omega_y k_d}{j\omega_y\left\{k_d + 2\zeta_y(\omega_y + \Delta\omega) + (\omega_y + \Delta\omega)^2/\tau_d\right\}} \right| = \frac{k_d}{k_d + 2\zeta_y(\omega_y + \Delta\omega) + (\omega_y + \Delta\omega)^2/\tau_d}. \tag{23}$$

Then the criterion of the scale factor uniformity in the gyroscope can be defined as

$$U_g \triangleq \frac{A_g - \min A_g'}{A_g} \le \delta_g, \tag{24}$$

where $\min A_g' = A_g\big|_{\Delta\omega \leftarrow \max\Delta\omega}$. Through elementary algebra, a condition for k_d is obtained as in (25) from (24).

$$k_d \ge a + b, \tag{25}$$

where

$$a = 2\zeta_y\left\{\frac{(1-\delta_g)}{\delta_g}\Delta\omega_{\max} - \omega_y\right\} \text{ and}$$

$$b = \frac{\omega_y}{\tau_d}\left\{\frac{(1-\delta_g)\Delta\omega_{\max}}{\delta_g}\left(2 + \frac{\Delta\omega_{\max}}{\omega_y}\right) - \omega_y\right\}.$$

3.4. Actuator saturation avoidance

In real application of designed control methods, the controller is realized using electrical components. Therefore, we have to consider the saturation of the actuator. If we use parallel-type control electrodes in the MEMS gyro-accelerometer, the control force f_c is calculated in terms of control voltage v_c as follows:

$$\begin{aligned} f_c(t) &= \varepsilon_0 N\frac{h}{g_0}\left(v_L^2 - v_R^2\right) \\ &= \varepsilon_0 N\frac{h}{g_0}\left\{\left(V_b + v_c(t)\right)^2 - \left(V_b - v_c(t)\right)^2\right\} \\ &= 4\varepsilon_0 N\frac{h}{g_0}V_b v_c(t), \end{aligned} \tag{26}$$

where ε_0 is electrical permittivity and N, h *and* g_0 are number, height, and initial gap of control electrodes, respectively. The v_L and v_R are applied voltages at the left and right side of the control electrodes. V_b is a bias voltage. If we let the controller $K(s)$ in Fig. 5 be $K(s)=k_vK'(s)$ shown in Fig. 6, and with the equation $u = f_c/m$, where m is the mass of the mechanical structure, then the gain of control force k_v will be equal to $k_v=4\varepsilon_0 NhV_b/(mg_0)$. The criterion that can avoid the saturation of the actuator have to reveal that the sum of the maximum outputs of the gyroscope and accelerometer should not exceed the voltage range of the circuit, which is expressed as follows:

$$v_{c\max} = \frac{A_{a\max}}{k_v}r_{a\max} + \frac{A_{g\max}}{k_v}r_{g\max} \le v_{range}, \tag{27}$$

where $r_{a\max}$, $r_{g\max}$ are the maximum linear acceleration input and the maximum Coriolis acceleration input values, respectively, and v_{range} is the voltage range of the control circuit. The $A_{g\max}$ is the maximum gain of the gyroscope and is given from (21) as

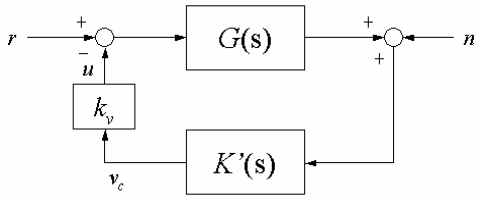

Fig. 6. Rebalance loop with modified controller.

$$A_{g\max} = k_d /(k_d + 2\zeta_{y\min}\omega_{y\min} + \omega_{y\min}^2/\tau_d). \quad (28)$$

The arranging of (27) in terms of k_i and k_d and solving the equation leads to the following condition.

$$\begin{aligned} k_i &\le \frac{\gamma k_d + \eta}{\alpha k_d + \beta} \quad \text{for } k_d > -\beta/\alpha, \\ k_i &\ge \frac{\gamma k_d + \eta}{\alpha k_d + \beta} \quad \text{for } k_d < -\beta/\alpha \end{aligned} \quad (29)$$

where

$$\begin{aligned} \alpha &= r_{a\max} + r_{g\max} - k_v v_{range}, \\ \beta &= \left(r_{a\max} - k_v v_{range}\right)\left(2\zeta_y\omega_{y\min} + \omega_{y\min}^2/\tau_d\right), \\ \gamma &= \omega_{y\min}^2\tau_i\left(v_{range}k_v - r_{g\max}\right), \text{ and} \\ \eta &= k_v v_{range}\omega_y^2\tau_i\left(2\zeta_y\omega_{y\min} + \omega_{y\min}^2/\tau_d\right). \end{aligned}$$

3.5. Stability margin of the loop

In addition to the performance condition, we have to consider the stability condition to decide the gain of the controller. Stability margin is an indicator of stability robustness. In this study, we focus on modulus margin as an indicator of stability robustness since the modulus margin is a more adequate stability margin that characterizes the robustness than gain and phase margin [18]. The modulus margin is the radius of the smallest circle with center (−1, 0) that is tangent to Nyquist plot, which is the same as the inverse of the maximum sensitivity function. The sensitivity function is given as

$$\begin{aligned} S(s) &= \frac{1}{1+L(s)} \\ &= \frac{s^3 + 2\zeta_y\omega_y s^2 + \omega_y^2 s}{s^3 + \left(2\zeta_y\omega_y + k_d\right)s^2 + \omega_y^2 s + k_i}, \end{aligned} \quad (30)$$

where $L(s) = G(s)K(s)$ and is assumed as $K(s) = \frac{k_i}{s} + k_d s$ for the conciseness of analysis. Note that the time constants of the controller, τ_i and τ_d are not included in (30) since their influence on the peak value of the sensitivity function is negligible. The modulus margin M is defined as

$$M = \inf_{\omega}\left|1 + L(j\omega)\right| = \inf_{\omega}\left|\frac{1}{S(j\omega)}\right|, \text{ which occurs at } \omega \approx \sqrt{\frac{k_i}{k_d + 2\zeta_y\omega_y}} \triangleq \omega_p \text{ by observing bode plots of the sensitivity function } S \text{ in the general operation of the sensor.}$$

Substitution of this into (30) leads

$$\begin{aligned} \frac{1}{M} &\approx \left|S(j\omega)\right|_{\omega=\omega_p} \\ &= \left|1 + j\frac{2\zeta_y\omega_y\sqrt{\left(k_d + 2\zeta_y\omega_y\right)k_i}}{\left(k_d + 2\zeta_y\omega_y\right)\omega_y^2 - k_i}\right| \\ &= \left|a + jb\right|. \end{aligned} \quad (31)$$

If we let the robustness condition be $M \ge M_{\text{spec}}$, where M_{spec} is a desired modulus margin specification, rearranging (31) with respect to k_i leads to

$$\begin{aligned} k_i^2 - 2\left(1 + \frac{2\zeta_y^2 M_{spec}^2}{1 - M_{spec}^2}\right)\left(k_d + 2\zeta_y\omega_y\right)\omega_y^2 \cdot k_i \\ + \left(k_d + 2\zeta_y\omega_y\right)^2\omega_y^4 \le 0. \end{aligned} \quad (32)$$

This is a second order equation of k_i. The solution is

$$\begin{aligned} k_i \le{}& \omega_y^2\left(k_d + 2\zeta_y\omega_y\right) \\ &\times\left\{\left(1 + \frac{2\zeta_y^2 M_{spec}^2}{1 - M_{spec}^2}\right) + \sqrt{\left(1 + \frac{2\zeta_y^2 M_{spec}^2}{1 - M_{spec}^2}\right)^2 - 1}\right\}. \end{aligned}$$

Assuming $\zeta_y << 1$, the condition for the k_i is approximately given as

$$k_i \le \omega_y^2\left(k_d + 2\zeta_y\omega_y\right)\left(1 + \frac{2\zeta_y M_{spec}}{\sqrt{1 - M_{spec}^2}}\right). \quad (33)$$

This result defines the relationship between k_d and k_i when the modulus margin is given, which is a first order linear equation.

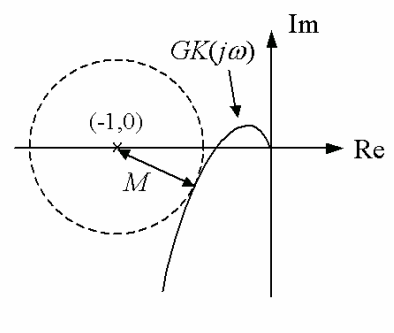

Fig. 7. Nyquist plot of GK and modulus margin.

3.6. Determination of the integral and derivative gains

From the condition of previous equations (10), (15), (19), (25), (29) and (33), we can determine the adequate control gain that satisfies all the conditions of performance and stability. The gray portion in Fig. 8 depicts the overlapped area of those inequality equations. All the points in the area are candidates of

the admissible control gain. In this case, we had better choose the smallest gain possible for smaller sensitivity function and noise reduction.

The area depends on performance condition and the mechanical parameters of the system. Fig. 9 shows the example of change of area as the resonant frequency of the structure is changed. If the overlapped area is not given, we have to lose the performance condition

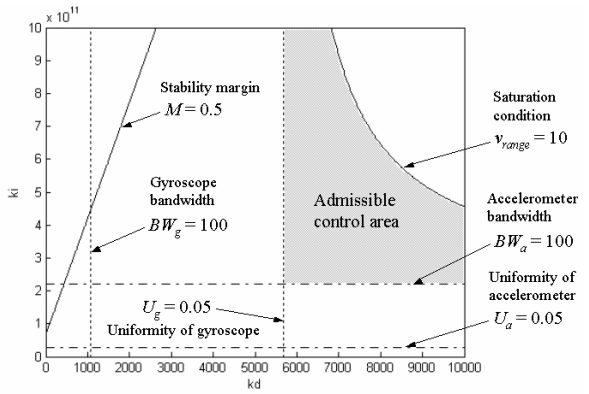

Fig. 8. A graph of control gain determination at ωy = 3 kHz and Qy = 100

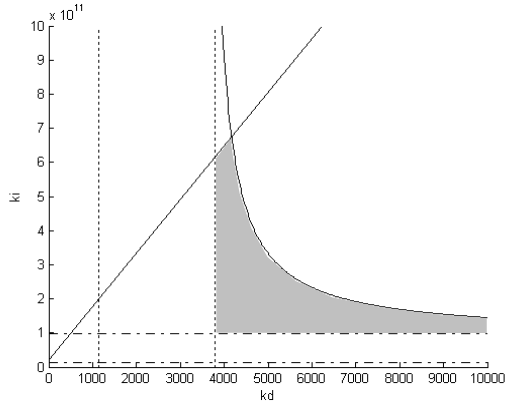

(a) ωy = 2 kHz.

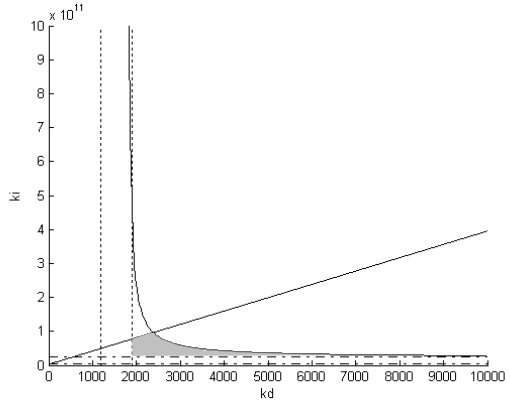

(b) ωy = 1 kHz.

Fig. 9. Change of graph at different resonant frequencies. The performance and stability conditions are same as those in Fig. 8.

or change the mechanical and electrical parameters of the system. The whole design procedure can be summarized as follows:

Step 1: Set the controller transfer function as (5) and determine the value of τ_i and τ_d such that $\tau_i << BW_a$ and $\tau_d > 3\omega_y$.

Step 2: Calculate the required range of k_i and k_d from the bandwidth and scale factor uniformity condition in Equations (10), (15), (19), and (25).

Step 3: Calculate the required range of k_i and k_d from the saturation avoidance and stability condition in Equations (29) and (33).

Step 4: Plot the calculated range of k_i and k_d in the 2D graph.

Step 5: Choose the appropriate values of k_i and k_d within the overlapped area of the plotted graph.

Step 6: Perform a simulation using the chosen values and check the performance and stability of the controller. If it is not satisfactory, repeat the procedure from Step 5.

4. SIMULATION RESULTS

Simulations using typical MEMS sensor parameters are performed to verify the performance of the designed controller. The parameter values of mechanical structure of the MEMS gyro-accelerometer are listed in Table 1. As shown in Table 1, there is a parameter variation in the mechanical structure for the simulation of robust performance. The resonant frequency of the drive mode is perturbed by 10% (±5%) and that of the sense mode is also perturbed by 10% in the drive mode frequency, which is called 'deviation' of resonant frequency. Perturbation ratio of the quality factor of the drive and the sense mode is set to 20% (±10%), which is the usual manufacturing error ratio of MEMS inertial sensors. The nominal value of drive mode is 1000 while that of sense mode is a lower value of 100 or ζ_y

Table 1. Mechanical parameters in MEM gyro-accelerometer.

Parameters			Value
Resonant frequency of drive mode	f_x	Max.	3.15 kHz
		Nom.	3 kHz
		Min.	2.85 kHz
Quality factor of drive mode	Q_x	Max.	1100
		Nom.	1000
		Min.	900
Resonant frequency deviation	Δf ($f_y = f_x + \Delta f$)	Max.	150 Hz
		Nom.	0
		Min.	-150 Hz
Quality factor of sense mode	Q_y	Max.	110
		Nom.	100
		Min.	90

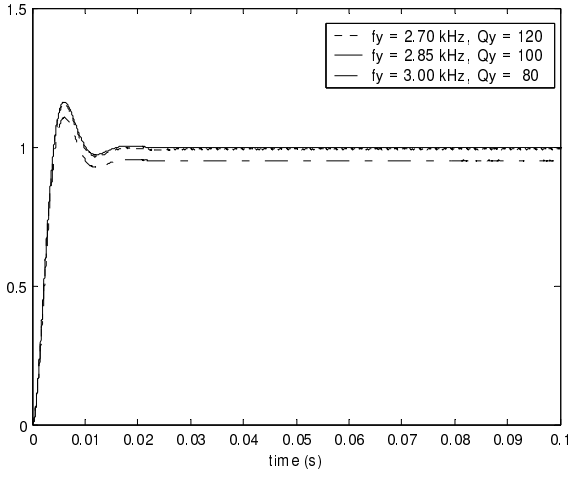

(a) fx = 2.85 kHz, Qx = 1100.

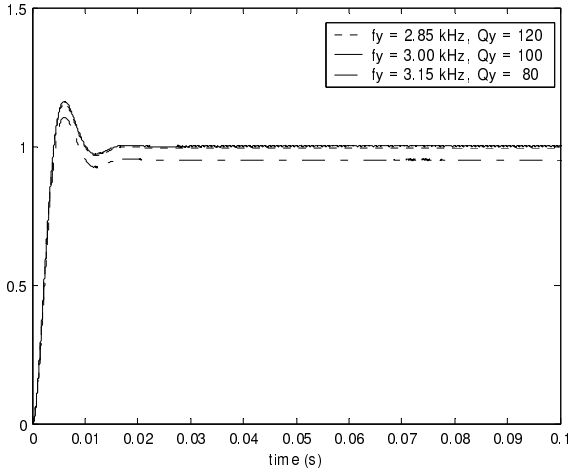

(b) fx = 3 kHz, Qx = 1000.

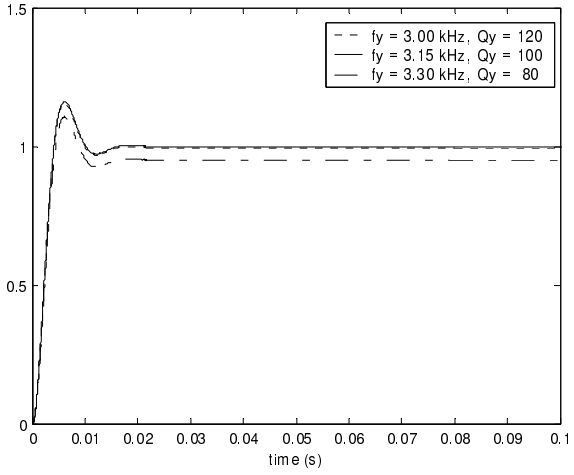

(c) fx = 3.15 kHz, Qx = 900.

Fig. 10. Simulated output of gyroscope under the perturbation of mechanical parameters by 10% of resonant frequency and 20% of quality factor for both dr ive and sense mode.

= 0.005 since the quality factor of sense mode directly affects the performance and uniform scale factor. The

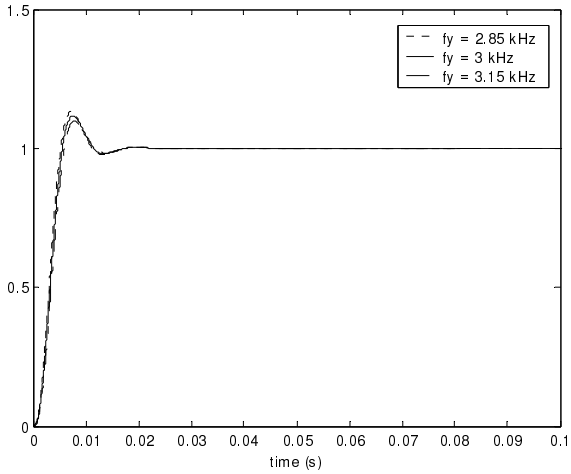

Fig. 11. Simulated output of accelerometer under the perturbation of resonant frequency by 10%.

times constants in the controller are set to be τ_i =20 and $\tau_d = 5\omega_y$.

The desired specification for the controller is assumed so that the modulus stability margin is kept to be greater than 0.5, bandwidth for gyroscope and accelerometer greater than 100 Hz, scale factor uniformity less than 0.05 for both gyroscope and accelerometer, and saturation voltage less than 10 volts with uncertainties as given in Table 1. Fig. 8 shows the range of gains k_d and k_i to satisfy the required specification or the controller. The shaded area is the region for the gains to satisfy all the required conditions. As is shown in Fig. 8, the conditions for accelerometer bandwidth, for uniformity of gyroscope, and for saturation voltage determines the admissible region for the control gains. The controller gains are chosen to be $k_d = 6\times10^3$ and $k_i = 3\times10^{11}$ according to the condition in Fig. 8, which includes a pickoff gain at capacitive sense circuit. The usual gain of pickoff circuit is 10^8~10^9, therefore, electrical gain of the controller in real circuit would be lower in order of 10^8~10^9.

Fig. 10 shows the simulation results of the gyroscope under the perturbation given in Table 1. The bandwidth is approximately calculated as $BW_g \approx 110$ Hz considering that the system order and rising time of the step response and the scale factor uniformity is less than 5% as required for the controller. The result for the accelerometer is shown in Fig. 11. The bandwidth is almost the same as that of the gyroscope. The scale factor uniformity is less than 0.5%, which is much better than the required condition of 5%. This is because the accelerometer bandwidth condition is much tighter than that for the uniformity of the accelerometer as presented in Fig. 8. These results demonstrate that the proposed design formulae can be effectively used to design controllers

for a gyro-accelerometer keeping the required performance over parameter variations.

5. CONCLUSION

In this paper, we presented a controller design method for a MEMS gyro-accelerometer to achieve good performance and robustness under parameter variations. Using the proposed scheme, a force rebalance loop was designed for robust performance and stability of the gyro-accelerometer with given performance specifications. The computer simulation results indicate that the controller with the proposed scheme achieves all the desired performance robustness specifications under parameter perturbations by 10% of resonant frequency deviation and by 20% of quality factor variation, demonstrating the usefulness of the proposed controller design scheme. The proposed method can be utilized for the design of the controller not only for the gyro-accelerometer but for each single-axis sensor of the gyroscope or accelerometer as well.

REFERENCES

[1] M. Lemkin, B. E. Boser, D. M. Auslander, and J. H. Smith, "A 3- axis force balanced accelerometer using a single proof-mass," *Proc. Transducers*, Chicago, IL, pp. 1185-1188, June 1997.

[2] K. Kwon and S. Park, "A bulk-micromachined three-axis accelerometer using silicon direct bonding technology and polysilicon layer," *Sensors and Actuators, A: Physical*, vol. 66, pp. 250-255, 1998.

[3] R. Toda, N. Takeda, T. Murakoshi, S. Nakamura, and M. Esashi, "Electrostatically levitated spherical 3-AXIS accelerometer," *Proc. of IEEE International Conference of Micro Electro Mechanical Systems*, pp. 710-713, 2002.

[4] T. Fujita, T. Mizuno, R. Kenny, K. Maenaka, and M. Maeda, "Two-Dimensional Micromachined Gyroscope," *Proc. of the 9th Int. Conf. on Solid-State Sensors and Actuators*, Chicago, USA, pp. 887-890, 1997.

[5] S. An, Y. S. Oh, K. Y. Park, S. S. Lee, and C. M. Song, "Dual-axis microgyroscope with closed-loop detection," *Sensors and Actuators*, vol. 73, pp. 1-6, 1999.

[6] T. Juneau, A. P. Pisano, and J. H. Smith, "Dual axis operation of a micromachined rate gyroscope," *Proc. of Transducers 97*, Chicago, vol. 2, pp. 883-886, June 1997.

[7] R. H. Hulsing, "MEMS inertial rate and acceleration sensor," *Proc. of IEEE PLANS '98*, pp. 169-176, 1998.

[8] J. H. Weng, W. H. Chieng, and J. M. Lai, "Structural design and analysis of micromachined ring-type vibrating sensor of both yaw rate and linear acceleration," *Sensors and Actuators A: Physical*, vol. 117, no. 2, pp. 230-240, 2005.

[9] T. Murakoshi, Y. Endo, K. Fukatsu, S. Nakamura, and M. Esashi, "Electrostatically levitated ring-shaped rotational gyro/ accelerometer," *Japanese Journal of Applied Physics*, vol. 42, pp. 2468-2472, 2003

[10] R. T. M'Closkey and A. Vakakis, "Analysis of a microsensor automatic gain control loop," *Proc. of American Control Conference*, San Diego, CA, pp. 3307-3311, 1999.

[11] Y. C. Chen, R. T. M'Closkey, T. Tran, and B. Blaes, "A control and signal processing integrated circuit for the JPL–Boeing micromachined gyroscope," *IEEE Trans. on Control System Technology*, vol. 13, no. 2, pp. 286-300, March 2005.

[12] R. Liu, B. Paden, and K. Turner, "MEMS resonators that are robust to process-induced feature width variation," *Journal of MEMS*, vol. 11, no. 5, pp. 505-511, October 2002.

[13] B. Kristiansson and B. Lennartson, "Robust tuning of PI and PID controllers: Using derivative action despite sensor noise," *IEEE Control Systems Magazine*, vol. 26, no. 1, pp. 55-69, Feb. 2006.

[14] S. Hara, T. Iwasaki, and D. Shiokata, "Robust PID control using generalized KYP synthesis," *IEEE Control Systems Magazine*, vol. 26, no. 1, pp. 80-91, Feb. 2006.

[15] M. Schlegel, J. Mertl, and M. Cech, "Generalized robustness regions for PID controllers," *Proc. of Process Control Conference*, pp. 108-114, 2003.

[16] W. K. Ho, C. C. Hang, and L. S. Cao, "Tuning of PID controllers based on gain and phase margin specifications," *Automatica*, vol. 31, no. 3, pp. 497-502, March 1995.

[17] Y. Q. Chen, K. L. Moore, B. M. Vinagre, and I. Podlubny, "Robust PID controller autotuning with a phase shaper," *Proc. of the First IFAC Symposium on Fractional Differentiation and its Applications*, Bordeaux, France, July 19-20, 2004.

[18] D. Garcia, A. Karimi, and R. Longchamp, "Robust PID controller tuning with specification on modulus margin," *Proc. of American Control Conference*, Boston, Massachusetts, pp. 3297-3302, June 30-July 2, 2004.

[19] W. T. Sung, C. Hyun, J. G. Lee, and T. Kang, "Design of an AGC driving loop in MEMS gyroscopes," *Proc. of ACA' 2007*, Toulouse, France, pp. 25-29, June 2007.

[20] K. Zhou, J. C. Doyle, and K. Glover, *Robust and Optimal Control*, Prentice Hall, 1996.

[21] W. T. Sung, S. H. Kim, J. G. Lee, and T. Kang,

"Development of a bulk-micromachined single crystal silicon gyroscope of wide operating range at atmospheric pressure," *Key Engineering Materials*, vol. 306-308, pp. 1259-1264, 2006.

[22] W. T. Sung, S. Sung, J. G. Lee, and T. Kang, "Design and performance test of a MEMS vibratory gyroscope with a novel AGC force rebalance control," *Journal of Micromechanics and Microengineering*, vol. 17, no. 10, pp. 1939-1948, Oct. 2007.

[23] J. Wu, *Sensing and Control Electronics for Low-Mass Low-Capacitance MEMS. Accelerometers*, Ph.D. Dissertation, Carnegie Mellon University, 2002.

[24] D. Stuart-Watson and J. Tapson, "A simple force balance accelerometer/seismometer based on a tuning fork displacement sensor," *Proc. the 1st African Control Conference*, Cape Town, South Africa, pp. 438-443, 2003.

[25] S. K. Sung, C. Hyun, and J. G. Lee, "Resonant loop design and performance test for a torsional MEMS accelerometer with differential pickoff," *International Journal of Control, Automation and Systems*, vol. 5, no. 1, pp. 35-42, 2007.

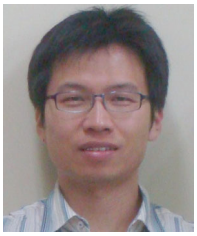

Woon-Tahk Sung received the B.S. degree from Hong-ik University in 2000 and the M.S. and Ph.D. degrees from Seoul National University in 2002 and 2007, respectively. His research interests include analog and digital control algorithm, as well as circuit design for microsystems using VCM, MEMS, and piezo actuators.

Taesam Kang is a Professor in the Department of Aerospace Information Engineering at Konkuk University, Korea. He received the B.S., M.S., and Ph.D. degrees from Seoul National University in 1986, 1988, and 1992, respectively. His current research areas are robust control theories and their applications, which include flight control, development of micro aerial vehicles, and MEMS inertial sensor develop-ment.

Jang Gyu Lee received the B.S. degree from Seoul National University, and the M.S. and Ph.D. degrees from the University of Pittsburgh in 1971, 1974, and 1977, respectively, all in Electrical Engineering. His research interests include gyroscope develop-ment, navigation systems, GPS, and filtering theory and its applications.